JOURNAL OF MATERIALS SCIENCE **35** (2000) 2279–2289

Interlayer structure of carbon fibre reinforced aluminium wires

E. PIPPEL, J. WOLTERSDORF
Max-Planck-Institute of Microstructure Physics, D-06120 Halle, Weinberg 2, Germany

M. DOKTOR
Austrian Research Centre Seibersdorf, A-2444 Seibersdorf, Austria

J. BLUCHER
Department of Mechanical Engineering, Northeastern University Boston, 360 Huntington Avenue, Boston, Massachusetts 02115, USA

H. P. DEGISCHER
Institute of Materials Science and Testing,Vienna University of Technology, Karlsplatz 13/E308, A-1040 Vienna, Austria

As the extent of the interfacial reactions controls the properties of metal matrix composites, the microstructural features and the chemical composition of the interlayers in aluminium wires reinforced with unidirectional carbon fibres (volume fraction app. 55%) have been investigated. High voltage and high resolution transmission electron microscopy of fibres, matrix, and interlayers, combined with analytical methods (electron energy loss spectroscopy and energy filtered microscopy) revealed a nanometre-sized C/Al interdiffusion layer and aluminium carbide needles or platelets of 10–50 nm thickness and 50–500 nm length in the matrix material, starting from the interlayer, the extension of which strongly correlates with the duration of melt contact. The observed interlayer phenomena impose restrictions to the process parameters, as by massive interface reactions the fibre strength is degraded, and the formation of brittle reaction products such as Al_4C_3 provides sites for initiation of fibre cracking and can cause composite failure. With a newly developed continuous process, which is capable of infiltrating endless products, the fibre/melt contact duration could be reduced to less than one second resulting in carbide formation lower than 0.2 wt% as confirmed by chemical analyses. So it was possible to achieve strength values of the composite wires that are as high as the theoretical prediction.

1. Introduction

Fibre reinforced metal matrix composites can be fabricated using liquid metal pressure infiltration processes, where fibre preforms (ceramic or graphitic) are infiltrated with molten metal under high pressure. The high pressure is required to compensate the non-wetting conditions existing between the reinforcement and the liquid metal like aluminium and magnesium based alloys. In the case of gas pressure infiltration the metal is forced into the fibre preform by an inert gas such as argon, and the pressure is typically in the range of 1 to 10 MPa. The extent of the chemical interaction between the liquid metal and the reinforcement depends on the constituents and on the contact duration. It can essentially deteriorate the composite properties due to fibre degradation and the formation of brittle reaction products at the interface which govern the failure mechanisms [1–4]. As, in general, the effectiveness of the fibre-reinforcement in metal matrix composites is strongly affected by the properties of the interlayers between fibre and matrix, some work was done to find out the optimum interlayer properties. For graphite fibre reinforced Mg/Al-alloys [2] as well as for boron fibre reinforced aluminium [5], it turned out that neither a very low nor a very high interface strength is favourable to the composite properties, rather the interface bonding must have an optimized value between these extremes which can be achieved by a moderate interface reactivity or correspondingly short reaction times. The usual cycle time of batch process units is in the order of minutes, depending on the mass of metal used for infiltration. For such long contact periods only a fraction of the theoretical strength potential of carbon fibre reinforced aluminium can be achieved due to carbide formation and fibre degradation [6, 7]. With a newly developed continuous gas pressure infiltration process this reaction time could be reduced to less than one second [8]. This process enables the efficient fabrication of carbon fibre reinforced aluminium wires which combine the high strength or large Young's modulus of the

fibres with the properties of the ductile metallic matrix. Moreover, the thermal expansion of the wires can be reduced to nearly zero and the high-temperature stability is noticeably improved with respect to the matrix metal. For these reasons, together with the low density and the electrical conductivity, these wires are predestined for high-tension power lines or reinforcements of cast components.

The paper is organized as follows: first we describe the process route of the wire fabrication, the macroscopic testing of the wires and the methods used for structural and chemical microanalysis. Then the results of the macroscopic and microscopic investigations are given followed by a summary of the interlayer phenomena observed in the different batches. Finally the mechanisms forming the interface reaction products and the resulting consequences on the properties of the composite wires are discussed.

2. Wire production and macroscopic testing

Fig. 1 shows a schematic sketch of the process route developed at Northeastern University, Boston. In a joint effort the production parameters for the chosen composite were developed and are shown in Table I for the selected specimens [8].

This process can be used to produce metal-matrix composite (MMC) wires with various combinations of metal matrices and reinforcements. The fibres are fed through an infiltration chamber where the gas pressure is applied. During the infiltration process the pulling speed of the fibres and thus of the wire can be varied from 1 to 15 m/min, i.e. the infiltration time is changing from 1.3 to 0.2 seconds for increasing pulling speed. The diameter of the reinforced aluminium wire is controlled by an orifice system. The wires investigated consist of a high purity aluminium matrix (99.99%), and unsized THORNEL P-25 fibres (pitch based) as reinforcement. Some of the fibre properties are: tensile strength of the fibre bundle 1.38 GPa; Young's modulus 159 GPa; diameter 11 μm; carbon assay $>$97% [9]. From single fibre tensile tests a tensile strength of 1.76 GPa was determined by applying Weibull statistics [10], which is more relevant for strength predictions of metal-matrix composites then the bundle strength. Tensile tests and aluminium carbide measurements have been performed to characterize the metal-matrix composite wire.

TABLE I Production parameters for the selected specimens

Specimen	A	B	C
Pulling speed [m/min]	2 to 4	1.8	8.4
Infiltration time [s]	1.2 to 0.6	1.3	0.3
Melt temp. [°C]	730	725	745
Infiltration pressure [MPa]	3.5	4.1	3.9
Av. tensile strength [MPa]	830	780	940
Carbide content [wt%]	—	0.36	0.14

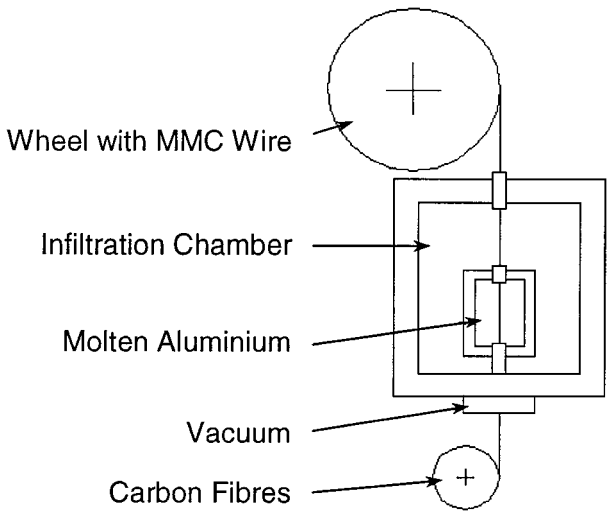

Figure 1 Scheme of the composite processing route.

The tests have been performed for different infiltration times and the tensile specimens were 102 mm long with a gauge length of 25 mm. The ends were fixed with epoxy adhesive in a steel tube. All tests were performed at room temperature using a standard Instron machine with a speed rate of 0.375 mm/min.

To evaluate the aluminium carbide content, the composite was dissolved in sodium hydroxide. The developed gas volume was measured and then analyzed in a gas chromatograph. Knowing the mass of the sample and the hydrogen and methane content of the gas, one can calculate the aluminium and aluminium carbide content with an accuracy of $\pm$0.02 wt%.

For the investigations presented here wires of h.p.Al/C-P25/55 (matrix/fibre/volume content of the fibres in %; h.p. means high purity, i.e. 99.99%) with about 1.4 mm in diameter and lengths of 200 m have been fabricated with production rates in the range of 1.8 to 8.4 m/min (infiltration time 1.3 to 0.3 s). The volume fraction of the fibres was about 55%.

3. Methods of interlayer microanalysis

Thin electron transparent samples of the composite wire specimens have been investigated down to atomic dimensions using high voltage (HVEM) and high resolution electron microscopy (HREM) including electron energy loss spectroscopy (EELS) and energy filtered transmission electron microscopy (EFTEM) which makes possible the imaging with inelastically scattered electrons of a defined energy range. Thus, the combination with appropriate computer equipment enables the selective mapping of a specific element with high spatial resolution (about 2 nm) within a few seconds.

The samples were prepared by cutting thin ($<$200 μm) slices, dimple-grinding to about 10 μm, and finally Ar-ion milling. This provides specimens for high resolution and energy filtered imaging of only a few nanometres in thickness and a tolerable surface roughness.

For the microstructural and nanochemical investigations we used the high voltage electron microscope Jeol-JEM 1000-06 run at 1000 kV, and the high resolution Philips CM 20 FEG field emission electron microscope, run at 200 kV. The latter was equipped with

a Gatan Imaging Filter (GIF 200), mounted below the microscope column. Besides EELS, this filter enables element or chemical-bond specific imaging (EFTEM). Filtered images and some HREM bright-field images were digitally recorded by a slow-scan CCD camera within the GIF 200. For image processing and EEL spectrum treatment the Gatan Digital Micrograph and ELP software, resp., loaded on a Power Macintosh 7200/75, were employed.

The chemical composition and the lateral distribution of the interface diffusion and reaction phenomena as well as of the carbide precipitates having in some cases dimensions of only a few nanometres cannot be imaged sufficiently well by methods of X-ray microanalysis: The spatial resolution is limited by the fluorescence phenomena in adjoining matrix areas, and the recording of appropriate X-ray maps takes too much time. Therefore, the carbides were analysed and imaged by the electron energy filter technique (EFTEM) yielding a two-dimensional elemental distribution.

This new favourable method in materials science which is based on the spectroscopy of inelastically scattered electrons (EELS) is explained by help of the EEL spectrum near the carbon K-edge shown in Fig. 2: First, an energy window ($\Delta E = 10$–30 eV) is inserted in the Gatan imaging filter (GIF) behind the characteristic energy loss edge of interest in the EEL spectrum (post-edge). With the selected electrons, a subsequent electron-optical system forms an image, which is digitized by a slow scan CCD camera. Because of the low specific signal in the EEL spectrum the background has to be removed by recording one or two additional images (pre-edge 1, 2) using the same energy window in positions directly in front of the edge onset (two or three window technique, resp.). The calculation of an element specific image is now possible by dividing the image behind the ionization edge by one image in front of it (ratio map), or by subtracting the background, modelled with the two pre-edge images based on an exponential law, from the post-edge image (elemental map). While the latter method results in a true element distribution the former leads to an improved signal-to-noise ratio and is only little affected by varying specimen thickness and diffraction contrast [11].

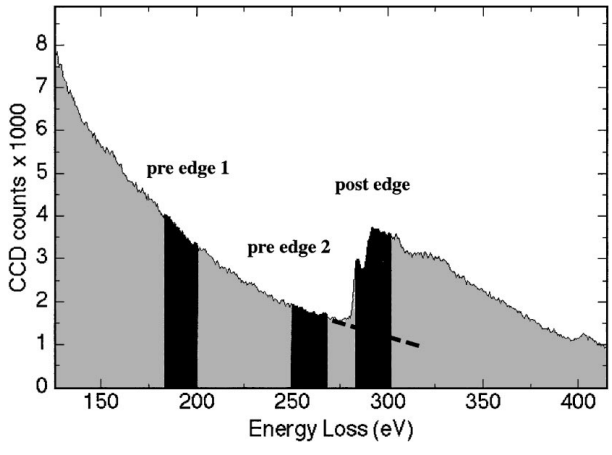

Figure 2 Energy window location for EFTEM (example: graphitic carbon, K-edge, $\Delta E = 30$ eV).

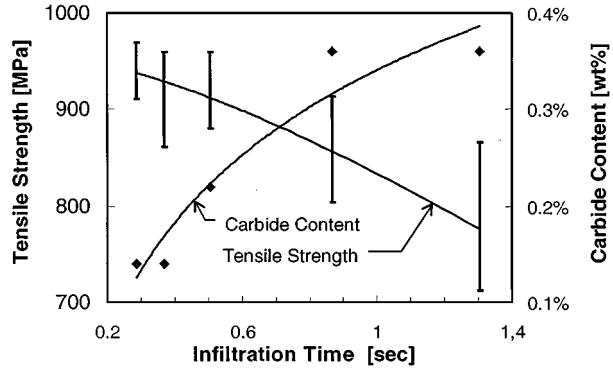

Figure 3 Tensile strength and carbide content in relation to the infiltration time of the composites.

Qualitatively, both methods should yield similar results, however.

4. Results of macroscopic characterization

The results of the tensile and carbide measurements can be seen in Fig. 3. The strength values vary between 710 and 970 MPa with higher values for shorter infiltration times. This is correlated to the amount of carbide formation decreasing with decreasing infiltration time. The strength of the continuous fibre reinforced aluminium wire is limited by damage mechanisms, which is concluded from the fracture surface of tensile specimens. Fig. 4a shows an almost flat fracture surface, correlated with lower strength due to more interface carbides causing brittle fracture. Whereas in Fig. 4b a pronounced fibre pull out can be seen yielding higher strength owing to less interface carbides, which allows crack branching.

5. Results of microstructural and nanochemical characterization

The HVEM overview image of Fig. 5 represents the typical fibre/matrix arrangement of all specimens investigated. The fibres are homogeneously distributed in the polycrystalline metal matrix the grain size of which is smaller with shorter contact times. The infiltration proceeds sufficiently; almost all the spacings between the fibres are filled up with matrix material. Even the smallest gaps down to a fibre distance of about 250 nm are infiltrated as shown in Fig. 6. Beyond this distance the surface tension of the melt prevents a further penetration, but the resulting uninfiltrated wedges along touching fibres revealed by TEM never exceeded a porosity of 3%.

Good bonding between fibres and matrix is still retained in the TEM foil as indicated by a ring of dislocations surrounding the fibres. The plastic deformation of the aluminium matrix occurs while cooling after infiltration and is caused by the thermal expansion mismatch of the constituents of the metal matrix composite. Fig. 7a shows faintly dislocations around the fibres forming a ring of more than 0.5 μm independently from the grain orientation. A quantitative evolution of the dislocations density is not informative due to the recovery occurring in the TEM foils thinner than a grain dimension.

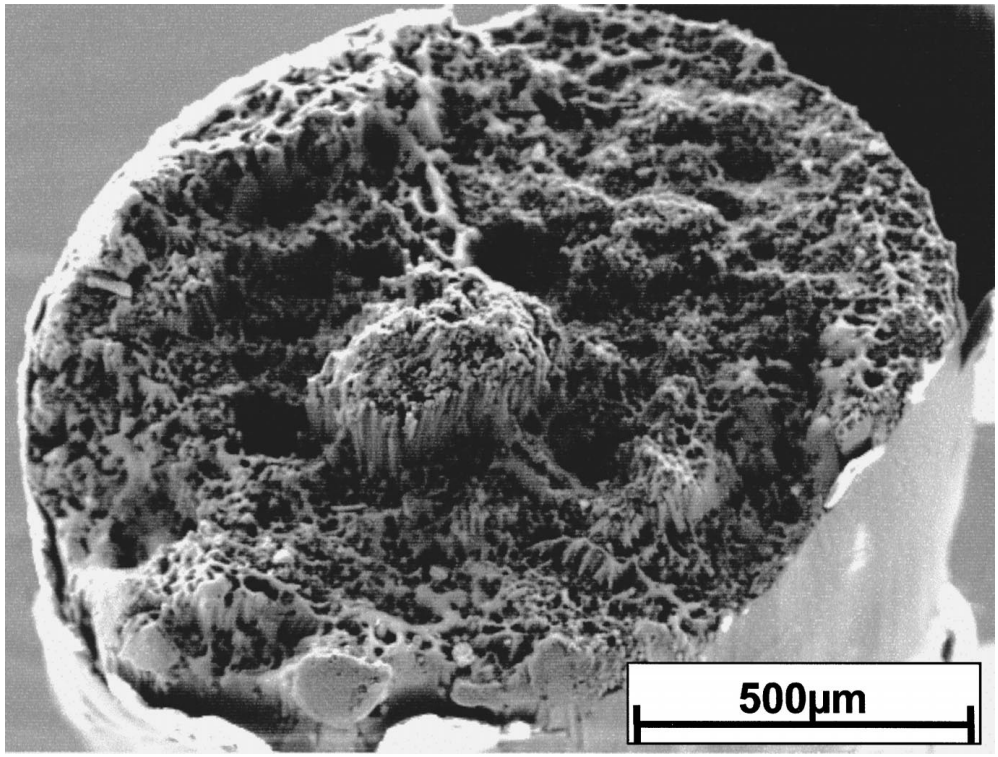

(a)

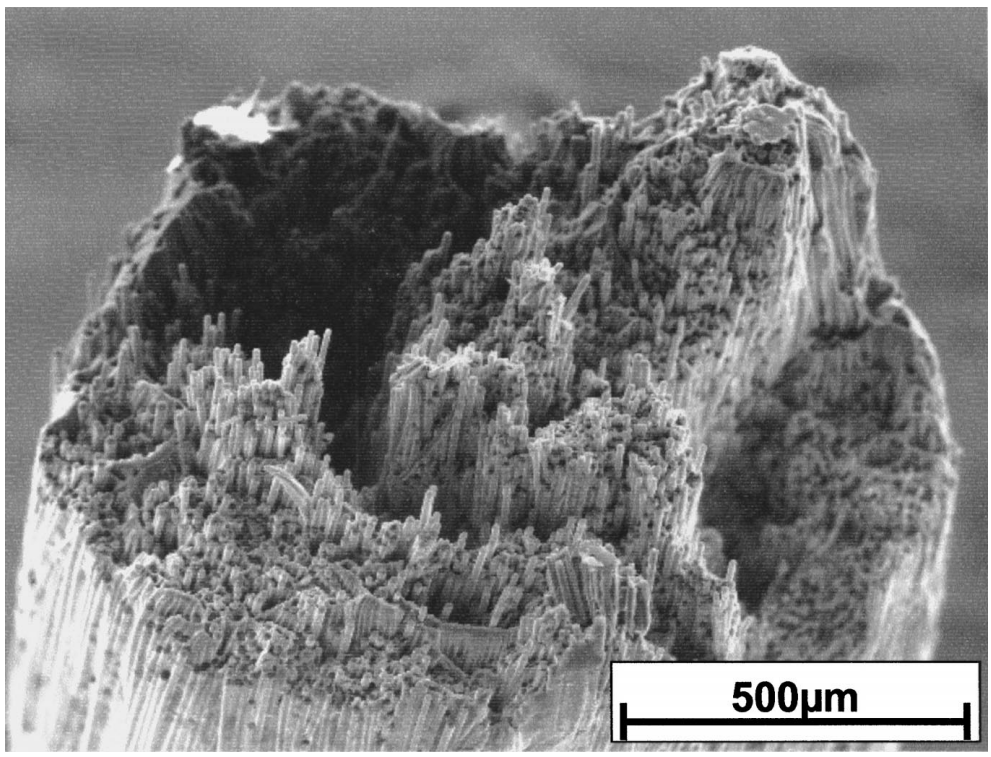

(b)

Figure 4 Fracture surfaces of tensile specimens with different production rates; (a) 1.3 sec; (b) 0.3 sec.

5.1. Carbide formation at interfaces

In general, the interlayers between fibre and matrix show the same structural peculiarities in all specimens, however, on different scales. As demonstrated in Fig. 8, the aluminium (right) is separated by a nanometre-sized ribbon of different contrast from the fibre (left). The atomic geometry of this layer and of the adjacent matrix and fibre regions can be seen in the lattice plane-resolved HREM image of Fig. 9. The atomic planes of the aluminium matrix (right) terminate directly at the surface of the interlayer, and the atomic structure of the surface-near fibre regions (left) bordering at the interlayer reveals a turbostratic arrangement of hexagonal basal planes of graphite which are aligned parallel to the interface. The interlayer of nearly amorphous structure between fibre and matrix has a thickness of 2–4 nm and consists of carbon enriched with aluminium as shown in the analytic Section 5.2, where also the Al and C

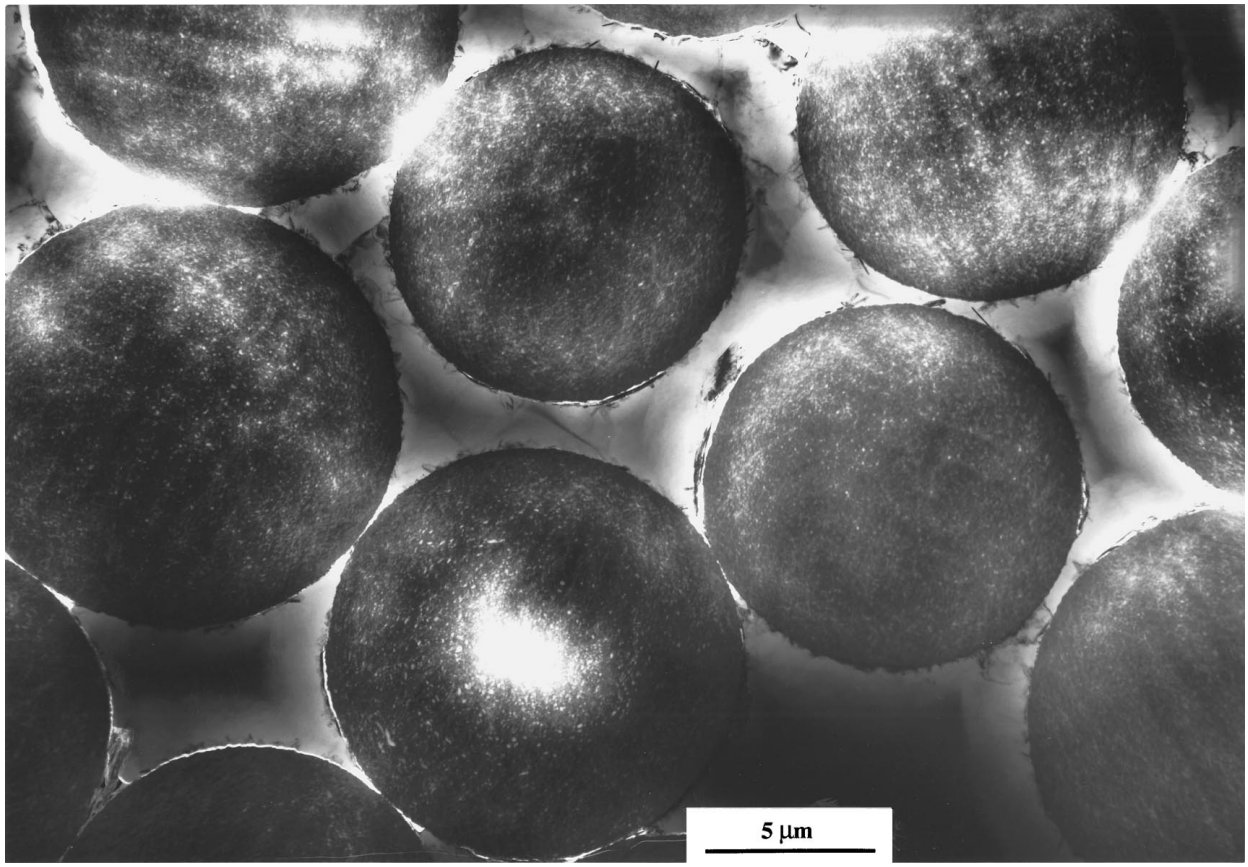

Figure 5 HVEM overview of the typical fibre/matrix arrangement.

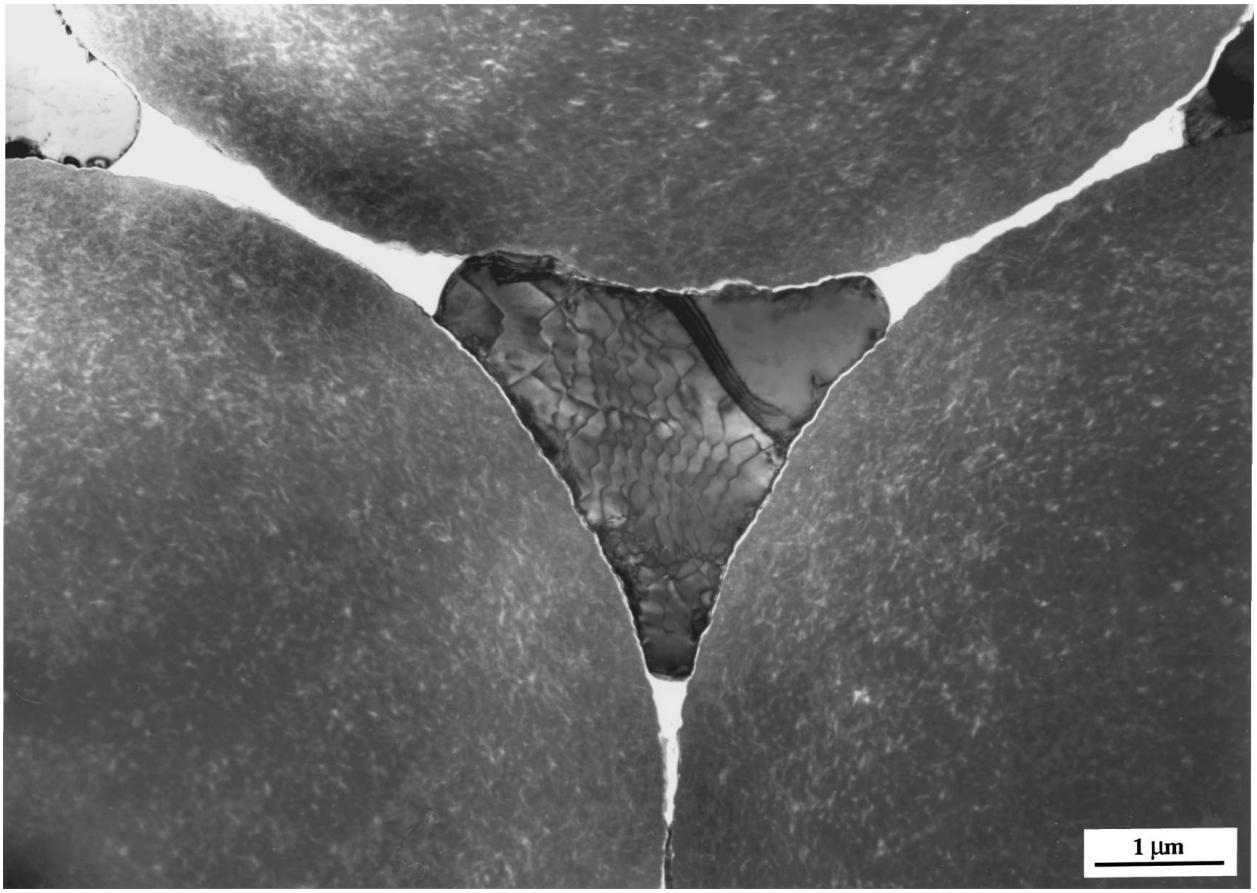

Figure 6 Triple junction between carbon fibres filled with aluminium (middle part) revealing the good fibre/melt infiltration.

(a)

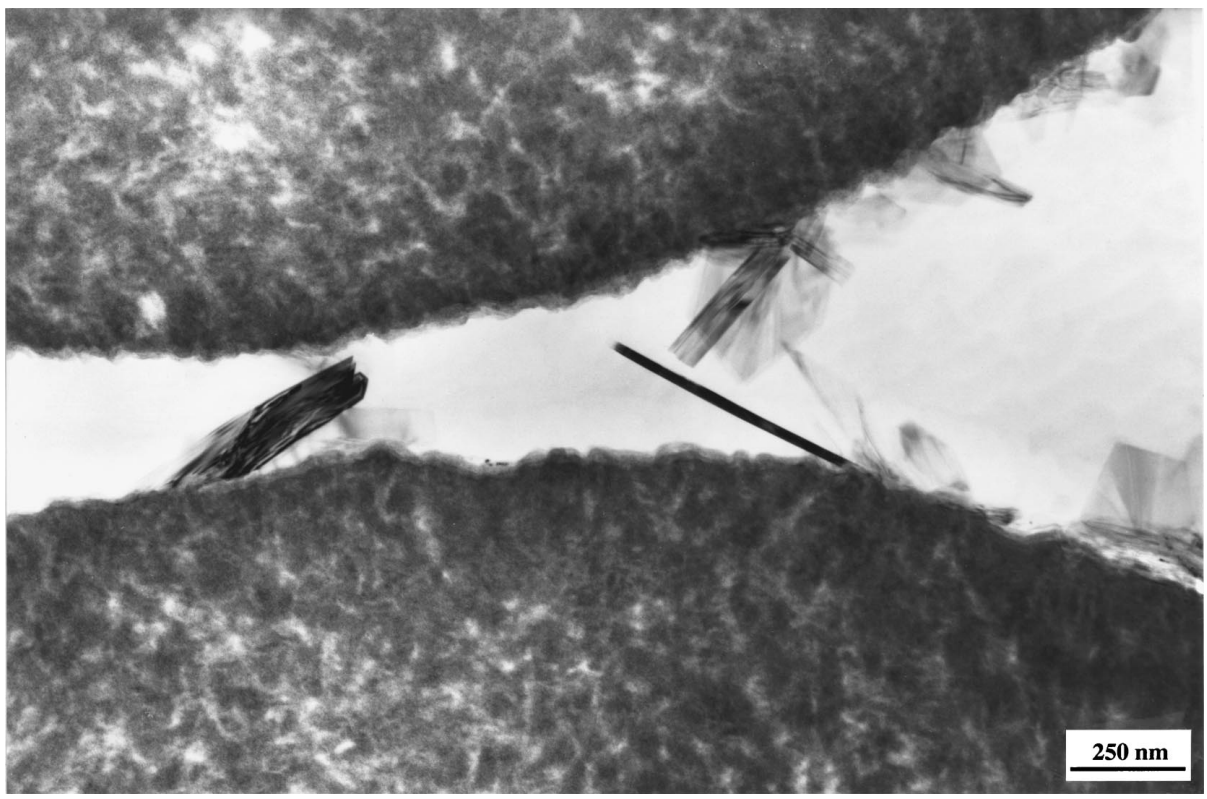

(b)

Figure 7 Different extent of carbide formation in specimens C (0.3 sec.) (a) and B (1.3 sec.) (b), (a) shows as well a faint ring of dislocations around the fibres.

diffusion profiles are discussed. Within this layer, small (1–2 nm) grains (encircled in Fig. 9) were sometimes observed having a lattice plane distance of approximately 0.26 nm. As this value corresponds to the ($1\underline{1}4$) lattice distance of Al_4C_3 these grains are assumed to represent nucleation centres for the formation of carbide plates.

The interlayers in all specimens contain needles or platelets of aluminium carbide, however , the extent of the carbide formation and the size of the precipitates

Figure 8 Nanometre-sized interlayer between fibre (left) and matrix (right).

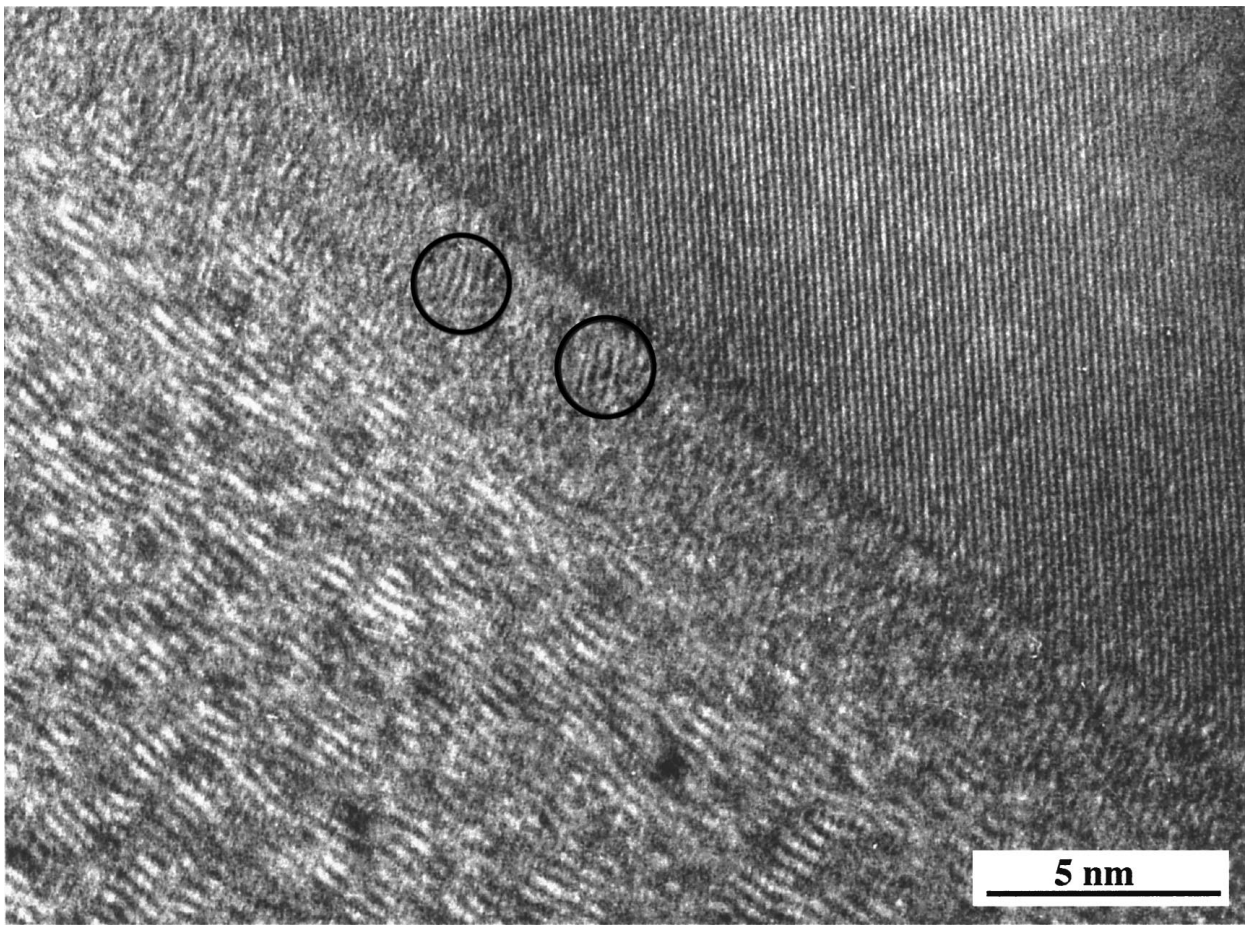

Figure 9 HREM image of the interface region between fibre (left) and matrix (right), encircled: aluminium carbide crystals.

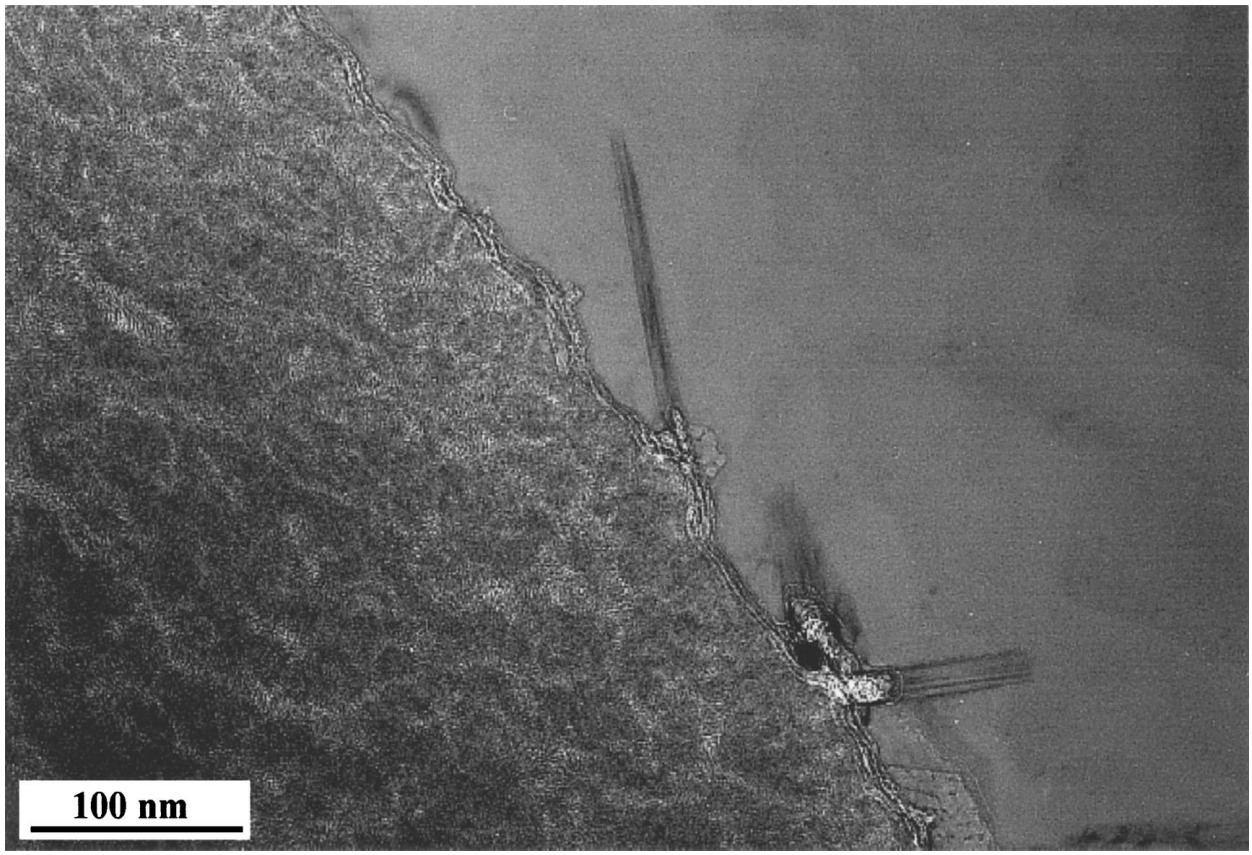

Figure 10 Carbide needles located at graphitic agglomerations.

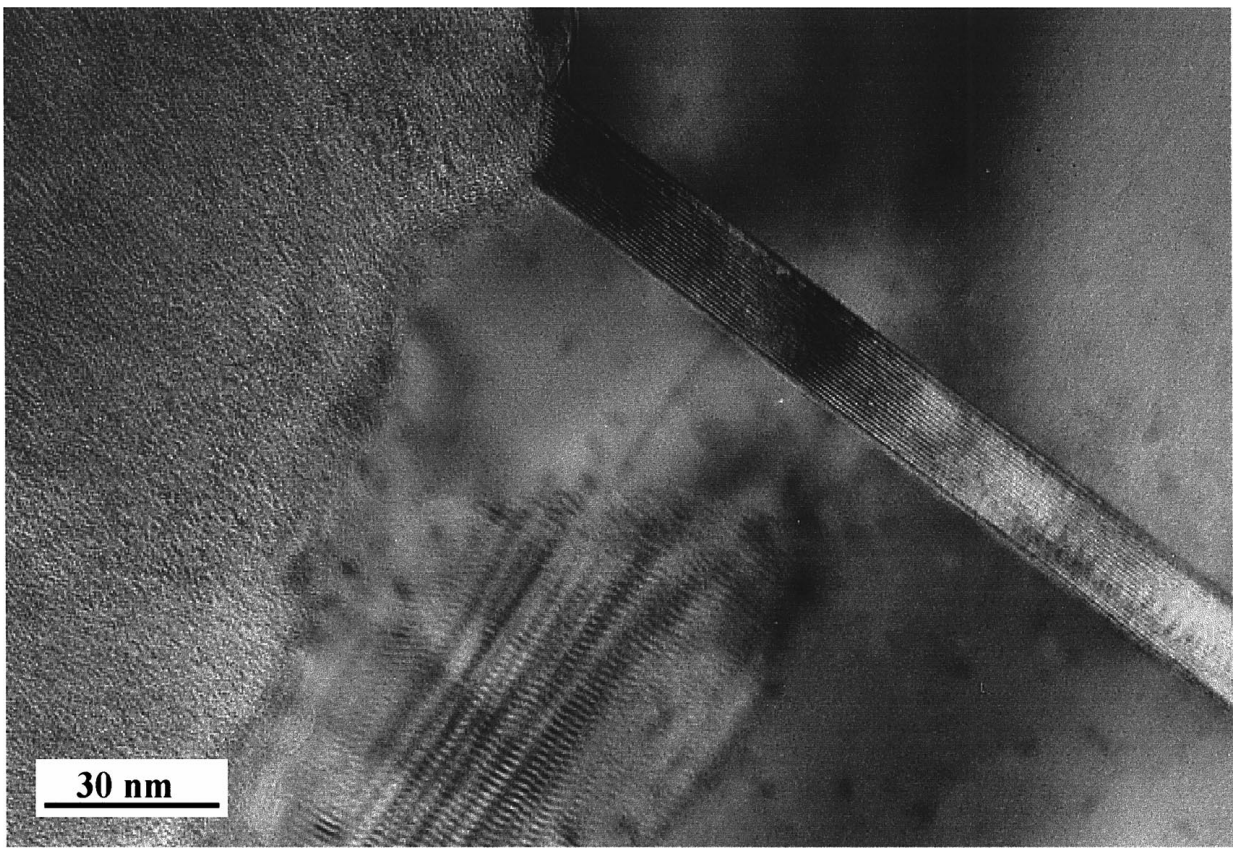

Figure 11 HREM image of a carbide needle.

is strongly dependent on the fibre/melt contact time as can be seen by comparing the Fig. 7a and b, which refer to specimens C (0.3 sec.) and B (1.3 sec.), respectively.

In principle, no morphological differences could be observed in differently sized precipitates. HREM techniques revealed the following general growth phenomena: The growth of the carbide needles or platelets starts immediately from the thin amorphous aluminium-containing surface layer of the fibre, mostly at local graphitic agglomerations (Fig. 10, fibre left) and, generally, at protruded parts of the fibre surface layer - possibly because of the better nucleation and growth conditions -, as demonstrated in the atomic plane resolved Fig. 11. The laterally extended carbides

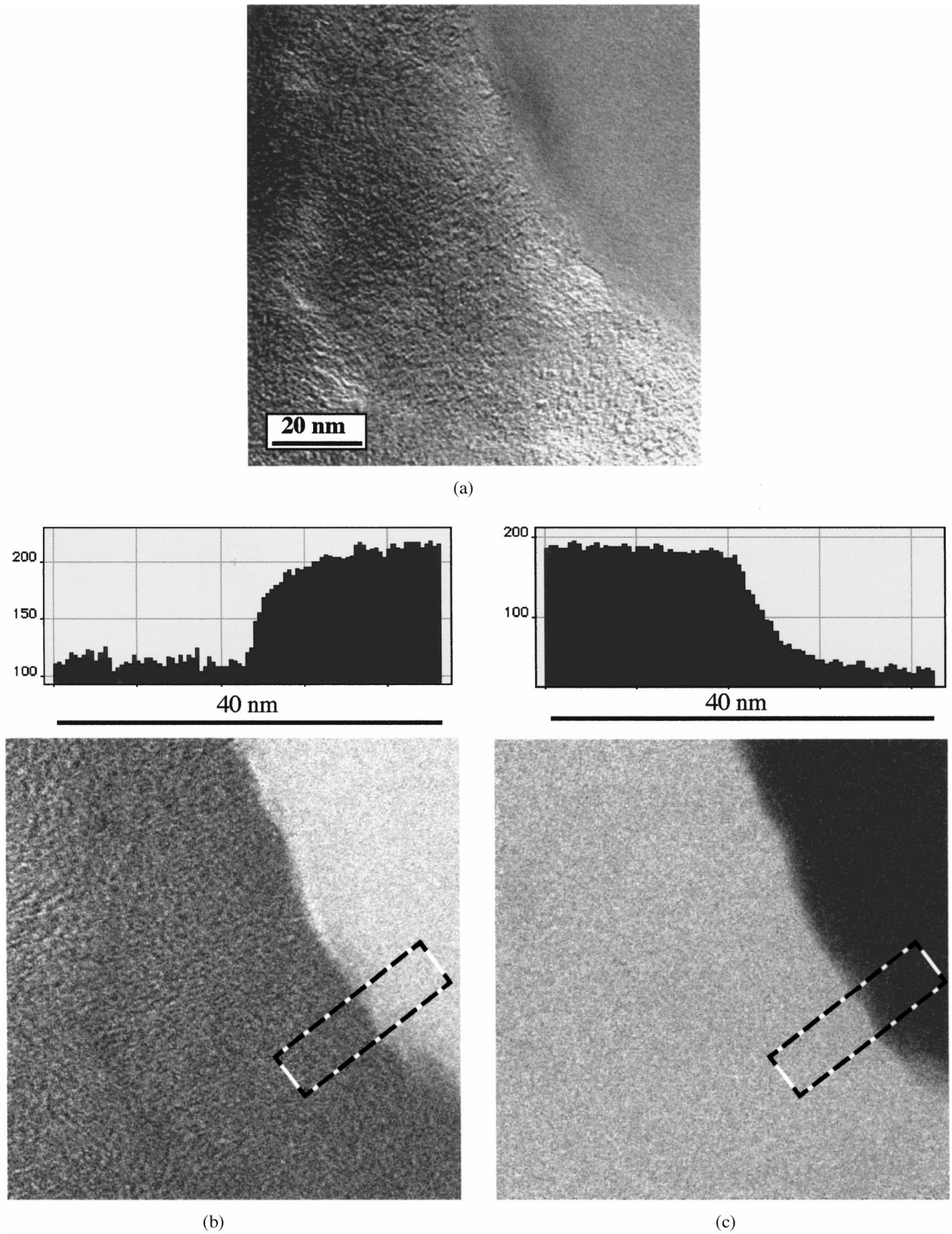

Figure 12 Interface composition between fibre (left) and matrix (right) with inserted intensity profiles of the marked area, (a) TEM bright field, (b) EFTEM Al-K edge (1560 eV), (c) EFTEM C-K edge (284 eV).

are single-crystalline, and the clearly visible atomic planes (003) of Al_4C_3 ($d = 0.83$ nm) are oriented parallel to the habit planes.

5.2. Nanochemical analyses

As a first result, EELS revealed with an accuracy of about 0.2% that no aluminium penetrated in the internal regions of the fibre, i.e. beyond the thin surface layer of about 2–4 nm. The distribution of elements in the interlayer region is shown in Fig. 12, using the three-windows elemental map technique described in Section 3. The bright-field image of Fig. 12a shows the region investigated (left fibre, right matrix); the mostly undisturbed area is analogous to that shown in Fig. 8. The corresponding elemental maps are recorded with the Al-K-edge at 1560 eV (Fig. 12b) and with the C-K-edge at 284 eV (Fig. 12c). It is evident that, apart from the narrow interlayer ribbon, that the aluminium is only existing in the matrix and the carbon only in the fibre. As the inserted intensity profiles in Fig. 12b, c show, the nanometre-sized interlayer is apparently composed of both, carbon and aluminium where almost no carbon has diffused into the Al matrix.

The chemical nature of the needle and plate-shaped precipitates is demonstrated in Fig. 13, again as a result of the three-window EFTEM technique. Fig. 13a is a HREM bright-field image showing an interlayer-near region containing such a needle; Fig. 13b and c represent the corresponding elemental maps recorded

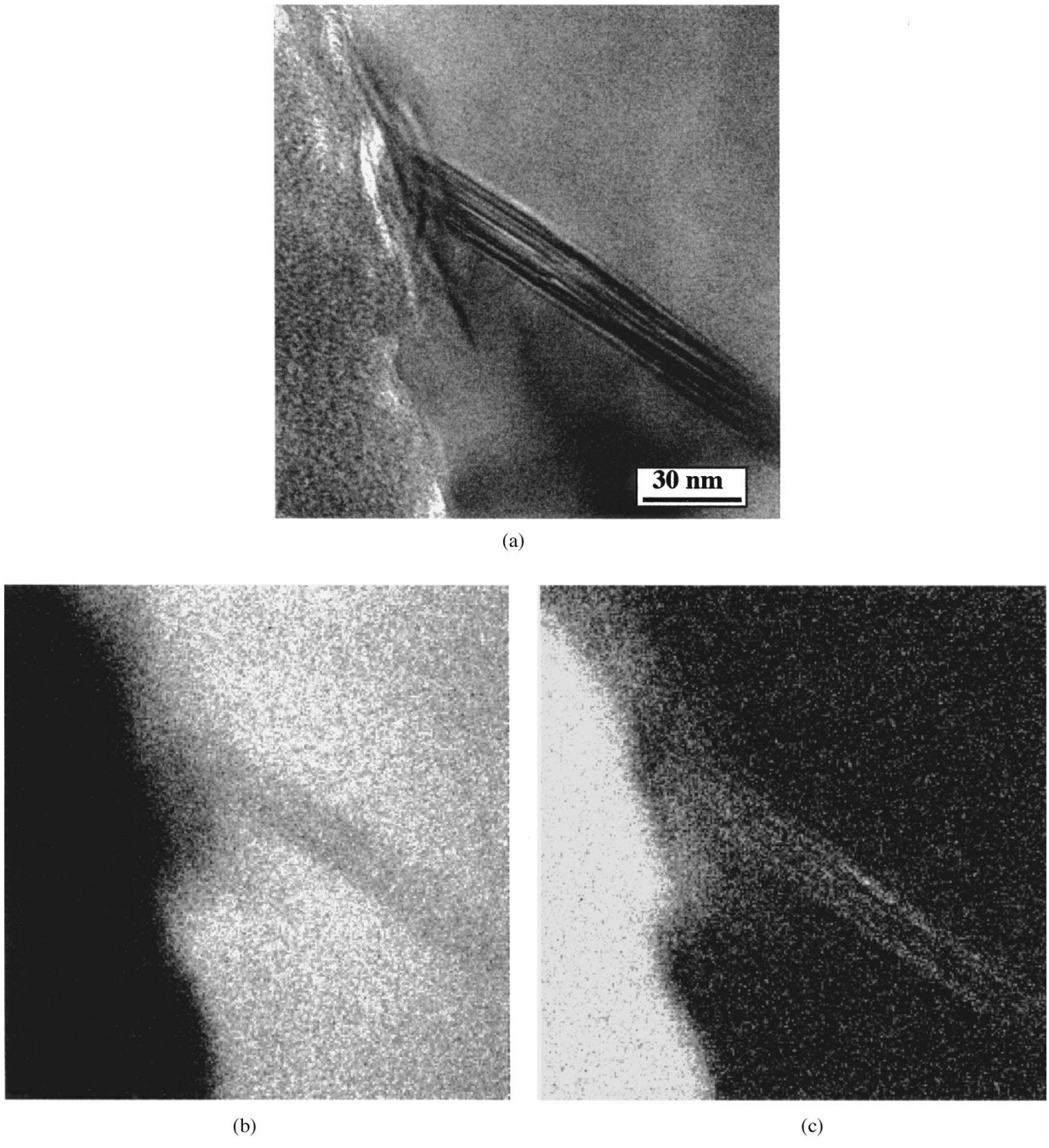

Figure 13 Carbide needle growing from the fibre (left) into the matrix (right), (a) TEM bright field, (b) EFTEM Al-K edge (1560 eV), (c) EFTEM C-K edge (284 eV).

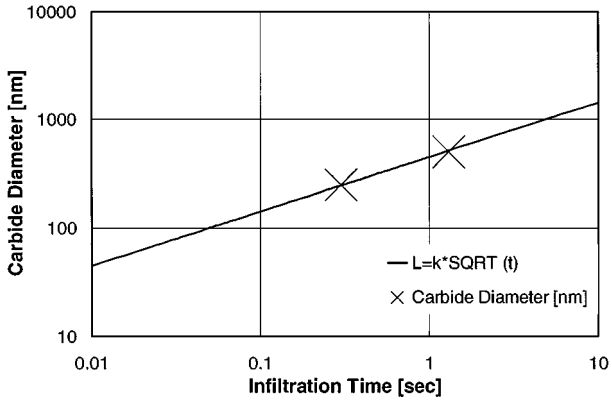

Figure 14 Comparison of the measured carbide lengths to the SQRT(t) law of precipitate growth (cf. text).

again with the Al-K-edge at 1560 eV and with the C-K-edge at 284 eV, respectively. Whereas the Al distribution exhibits a distinct aluminium depletion within the needle structures the carbon map shows an enrichment at corresponding places within the otherwise carbon-free matrix.

6. Conclusions

With the continuous infiltration process high quality MMC's could be produced even with extremely non-wetting constituents like carbon fibres and aluminium. The achieved infiltration quality is very good in spite of the short infiltration time (<3% porosity). This short fibre/melt contact time enabled a surprisingly strong reduction of carbide formation. Batches of 200 m infiltrated aluminium wire were achieved limited only by the amount of aluminium in the infiltration chamber. As carbon fibres and molten aluminium are very reactive, the notch effect of carbide needles decreases the tensile strength for longer fibre/melt contact times. High strength values could be realised with a carbide content less than 0.2 wt%.

The microstructural and nanochemical observations suggest that, according to the findings in [2, 3] and the observations in [12], the shape of the carbide precipitates is controlled on the atomic scale by the action of two different growth mechanisms: In directions normal to the atomically-flat interface between the metal matrix and the needle or platelet the carbide crystal grows by an interface-controlled ledge mechanism, which requires a multiple two-dimensional nucleation or a spiral growth mechanism. However, the atomically-rough interface at the tip of the needle or the edge of the platelet moves in a continuous diffusion-controlled growth mode, which is determined by the diffusion rates of the reaction partners. As the diffusion-controlled growth process is several times faster than the interface-controlled one, the observed needle or plate-shaped morphology of the carbide precipitates results.

The length of the carbides measured in the TEM micrographs is plotted in a double logarithmic diagram as shown in Fig. 14. Although only two different contact times were investigated the tendency of growth seems to coincide with a square root law [13] confirming the described growth mechanism.

From these analytical results together with the observed lattice distance (cf. Fig. 11) the conclusion can be drawn that the interlayer precipitates are aluminium carbide. Fig. 13 also reveals a carbon enrichment in the matrix at those places where the carbide precipitates start to grow (cf. Fig. 10). This is an almost general phenomenon in these composites, probably connected with the above described growth mechanism of the needles and platelets.

References

1. S. SURESH, A. MORTENSON and A. NEEDLEMAN, "Fundamentals of Metal-Matrix Composites" (Butherworth-Heinemann, 1993) p. 52.
2. A. FELDHOFF, E. PIPPEL and J. WOLTERSDORF, *J. Microscopy (London)* **185** (1997) 122.
3. *Idem., Philos. Mag. A* **79** (1999) 1263.
4. H. D. STEFFENS, B. REZNIK, V. KRUZHANOV and W. DUDZINSKI, *J. Mater. Science* **32** (1997) 5413.
5. M. K. SHORSHOROW, L. E. GUKASJAN and L. M. USTINOV, *J. Comp. Mater.* **17** (1983) 527.
6. H. P. DEGISCHER, P. SCHULZ and W. LACOM, *Key Engineering Materials* **127/131** (1997) 99.
7. W. LACOM, H. P. DEGISCHER and P. SCHULZ, *ibid.* **127/131** (1997) 679.
8. M. DOKTOR, H. P. DEGISCGER and J. BLUCHER, in Proc. SAMPE Europ. Conf., 1998, p. 555.
9. Amoco, Sheet of typical Properties of Thornel Pitch Based Fibers, Amoco Corporation Chicago Illinois, 1996.
10. M. DOLEZAL, "Einzelfaserzugversuche," Forschungsbericht, Technische Universität Wien, August 1998.
11. F. HOFER, P. WARBICHLER and W. GROGGER, *Ultramicroscopy* **59** (1995) 15.
12. M. GU, H. YANG, W. JIANG and G. ZHANG, *Adv. Composite Mater.* **5**(2) (1996) 119.
13. T. H. COURTNEY, in Proc. Int. Conf. on Solid→Solid Phase Transformations, 1981, p. 1057.

Received 8 December 1998
and accepted 1 November 1999